Sensors and Actuators A 179 (2012) 62–69

Contents lists available at SciVerse ScienceDirect

Sensors and Actuators A: Physical

journal homepage: www.elsevier.com/locate/sna

Flexible microfluidic normal force sensor skin for tactile feedback

Ruben D. Ponce Wong[a], Jonathan D. Posner[b], Veronica J. Santos[a,*]

[a] Mechanical and Aerospace Engineering, Arizona State University, Tempe, AZ, USA
[b] Mechanical Engineering, Chemical Engineering, University of Washington, Seattle, WA, USA

ARTICLE INFO

Article history:
Received 13 October 2011
Received in revised form 5 February 2012
Accepted 14 March 2012
Available online 29 March 2012

Keywords:
Capacitive sensor
Conductive fluid
Flexible sensor
Microfluidic force sensor
Sensor skin
Soft lithography

ABSTRACT

Robotic applications often require robust tactile sensing capabilities on curved surfaces, such as artificial fingertips. Flexible tactile sensors could be conformally wrapped around curved digits and could enhance grip by cushioning impacts and increasing the effective contact area during grasp. Flexible microfabricated devices that use thin film or solid electrical components are susceptible to failure due to cracking and fatigue. Conductive fluids have been used as transduction media, electrical connections, and in resistance-based pressure and bend sensors. In this work, a flexible and multilayer capacitive microfluidic normal force sensor is developed with a 5×5 taxel array. The sensor uses liquid metal-filled microfluidic channels as the capacitive plates and conductive interconnects. The sensor is microfabricated using soft lithography microfabrication techniques and consists of multiple layers of PDMS microchannels filled with the liquid metal alloy Galinstan and air pockets that modify the mechanical and electrical properties of the sensor. A single taxel is calibrated for normal forces ranging from 0 to 2.5 N, is shown to provide repeatable measurements of static uniaxial loads, and follows the loading and unloading phases of low-frequency dynamic loads (0.4–4 Hz). The sensor prototype has a spatial resolution on the order of 0.5 mm, performs reliably when wrapped around a surface having a curvature similar to that of a human finger ($1.575\ cm^{-1}$), and has been shown to tolerate curvatures as high as $6.289\ cm^{-1}$. The deformable liquid capacitive plates and heterogeneous PDMS-air dielectric medium can be designed to tune the sensor's sensitivity and range. The sensor prototype provides greater sensitivity at low loads, a feature which can be exploited for robotic applications in which light touch is important.

1. Introduction

There are three primary sensing modalities employed in microelectromechanical systems (MEMS) force sensors: resistive, piezoelectric, and capacitive [1]. Resistive sensors detect mechanical stimuli by producing changes in resistance. Traditional high sensitivity, resistive strain gauges typically have issues such as fragility and low flexibility. Recently, some of the existing limitations have been addressed, for instance, with the development of conductive polymer composites [2–4]. Piezoelectric sensors generate voltage as applied forces are measured. Piezoelectric composites are flexible and chemically resistant but inappropriate for static loading and prone to output signal drift. Capacitive sensors, the focus of the present work, typically consist of pairs of plates whose capacitance is increased as the distance between opposing plates decreases or the permittivity of the dielectric medium between the plates increases. Capacitive sensors offer advantages such as high sensitivity, tunable spatial resolution when used in an array configuration [1], and a simple, well-known governing equation. Electrical capacitance depends on the geometry of and distance between the electrodes and dielectric properties of the material between the electrodes.

1.1. Capacitive sensors

For many applications, capacitive sensors are created by embedding conductive metal plates in flexible materials such as the polydimethyl siloxane (PDMS) polymer. The conductive plates are typically created using metal deposition techniques such as evaporation [5,6], electroplating [7], or sputtering [8]. Although the polymeric packaging is relatively robust to mechanical deformations and chemical degradation, the conductive plates and interconnects are susceptible to failure due to fractures and fatigue. Even a small crack in a plate or connect can result in the irreparable loss of electrical connectivity and failure of the sensor [9]. Fabrication of curved, doped nano-ribbons that can withstand significant deformation [10] and the deposition of spiral copper wire around a nylon wire that elongates when stretched [11] have been used to provide electrical connections in flexible substrates.

* Corresponding author at: Arizona State University, 501 E. Tyler Mall, ECG 301, MC 6106, Tempe, AZ 85287-6106, USA. Tel.: +1 480 965 3207; fax: +1 480 727 9321.
E-mail addresses: Ruben.Poncewong@asu.edu (R.D. Ponce Wong), jposner@uw.edu (J.D. Posner), Veronica.Santos@asu.edu (V.J. Santos).

0924-4247/$ – see front matter © 2012 Elsevier B.V. All rights reserved.
doi:10.1016/j.sna.2012.03.023

Capacitive sensors have sensitivity and tunable spatial resolution [1]. Arrays of capacitors have been used for a wide range of applications. Capacitance-based micro tactile sensor arrays are capable of detecting mN forces with negligible cross-talk between sensing elements, although hysteresis can be an issue [12]. A macro-scale pressure sensor made of fabric detected pressure fields with magnitudes of hundreds of fF capacitance spread around a 1 m^2 area [13]. A sensor capable of measuring phase fraction distribution of two-phase flows via permittivity variations was developed to distinguish between different types of dielectric media between the capacitor plates [14]. A tactile sensor capable of measuring normal and shear forces was created by depositing an array of gold thin films in PDMS and using 2×2 taxels as a single sensing unit [7,15].

1.2. Fluids in MEMS sensors

Fluids have been integrated into a variety of MEMS sensors for different applications. For instance, a vibration sensor was developed which had chambers filled with a NaCl solution [16]. Mechanical vibrations induced motion of the electrolyte's ions, allowing the measurement of vibrations over a wide range of frequencies. For tactile sensing, a sensor was created by filling microchannels with a NaCl solution [17]. Mechanical deformation applied pressure to the reservoirs, displaced fluid, and produced measurable changes in resistance. A macroscale fluid-based tactile sensor called the BioTac (SynTouch, Los Angeles, CA) uses fluid as a transduction medium for both electric current and mechanical vibrations [18]. This multimodal sensor consists of an elastomeric skin that has been inflated away from a rigid, fingertip-shaped core by a weakly conductive fluid [19]. An array of impedance electrodes embedded in the rigid core is used to measure changes in impedance as the fluid flowpath is altered by mechanical deformation. A hydrophone is used to measure vibrations at the skin-object interface. Each of these three sensing devices utilizes fluids encapsulated by elastic materials.

Recently, fluids have been used as wires to connect sensing elements with external circuitry. A liquid metal alloy called Galinstan has been used in MEMS devices to create robust wire paths capable of being bent, twisted, and stretched. Galinstan-filled microchannels enabled the powering of LED lights despite the bending and twisting of the device [20]. In another application, a stretchable force and temperature sensor was created with carbon nanotubes and Galinstan electrical connections embedded in PDMS [21]. Galinstan is a fairly conductive (0.435 Ωm electrical resistivity [22]) fluid created by Geratherm (Geschwenda, Germany) for use in thermometers as a nontoxic substitute for mercury [23]. Galinstan is a eutectic metal alloy composed of gallium, indium, and tin [22]. The voltammetric [22] and electromagnetic [24] properties of this relatively new compound have been recently established. A eutectic metal alloy composed of only gallium and indium (eGaIn) has been used in the design of a pressure sensor [25] and bend sensor [26,27,45]. A PDMS skin having microchannels filled with eGaIn was wrapped around a human finger. Deformation-induced changes in resistance of the fluidic electrical circuit allowed for the measurement of joint angles as the finger was bent.

1.3. A capacitive microfluidic normal force sensor

Tactile sensing is a field of great interest due to its potential impact on robot-assisted surgery and robotic grasp and manipulation, among other applications. In many cases, visual and acoustic feedback alone does not provide the information necessary for decision making. A classic case is that of an amputee who accidentally crushes or drops an object with his prosthetic hand due to inadequate tactile information about the hand-object interaction. Many review articles have discussed the complexity of the sense of touch and the many challenges that remain for artificial touch sensors [1,28,29]. Some of the sensor design requirements for robotic applications include robustness, sensitivity, fine spatial resolution, fast dynamic response, and flexibility [29].

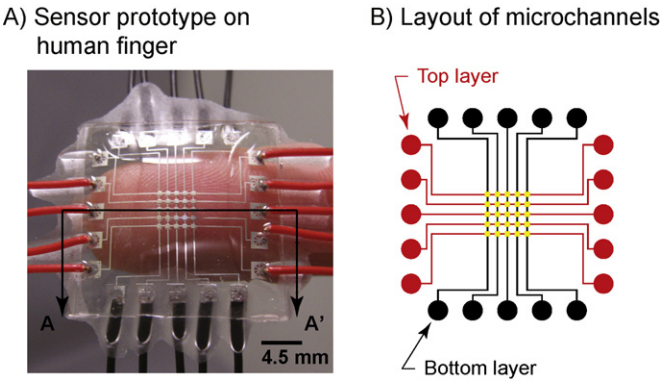

Fig. 1. Capacitive microfluidic normal force sensor skin. (A) A completed prototype shows the Galinstan embedded within the transparent PDMS. The 2D schematics in Fig. 2 correspond to the cross-sectional view at A–A′ (black line). (B) Wire paths from the top half of the sensor run horizontally (red) while those from the bottom half run vertically (black). The square capacitive taxels (yellow) represent the overlapping areas of the wire paths from both halves of the sensor. (For interpretation of references to color in this figure legend, the reader is referred to the web version of this article.)

PDMS-based capacitive tactile sensors have been developed to measure normal forces [2,7,12] and shear forces [15], to determine the elasticity of a contacted object [30], and to distinguish between different types of textures [31]. For MEMS and microfluidic applications, PDMS offers advantages such as non-toxicity, high degree of flexibility, chemically inert nature, simple processing techniques, low cost, and impermeability to liquids [32–35]. Thus, PDMS provides protection from the environment for the embedded sensor electronics. The existing PDMS-based tactile sensors use embedded solid metal films [7,12,15,30,31] or carbon nanotubes [2] in a protective PDMS material. These designs are prone to failure when deformed, for example around a robotic finger, and are therefore challenging to implement in robotic applications where conformal wrapping of curved surfaces or robustness to repetitive deformation is necessary.

In this work, we present a flexible, capacitive, microfluidic sensor for normal force sensing with microchannels filled with Galinstan that serve as both the flexible wire paths and the conductive metal plates that make up the capacitive sensing units. Novel features of the sensor include its deformable capacitive plates and heterogeneous, deformable dielectric medium. The prototype has a 5×5 array of individually addressable 0.5 mm × 0.5 mm taxels. The liquid metal-filled microfluidic channel design ensures the robustness of the sensor as there are no solid components that can crack and fail. The multilayer design allows for nonlinear tuning of the sensor response to the desired load. We present the sensor's spatial resolution and quantify the response of the capacitive sensor on flat and curved surfaces. Details of the sensor's design, fabrication, calibration, validation, and overall functional assessment are presented in this work to show the potential of using conductive fluids for sensor electronics.

2. Methods

2.1. Prototype fabrication

The capacitive, microfluidic sensor (Fig. 1A) is fabricated using soft lithography and consists of two materials: a flexible elastomer

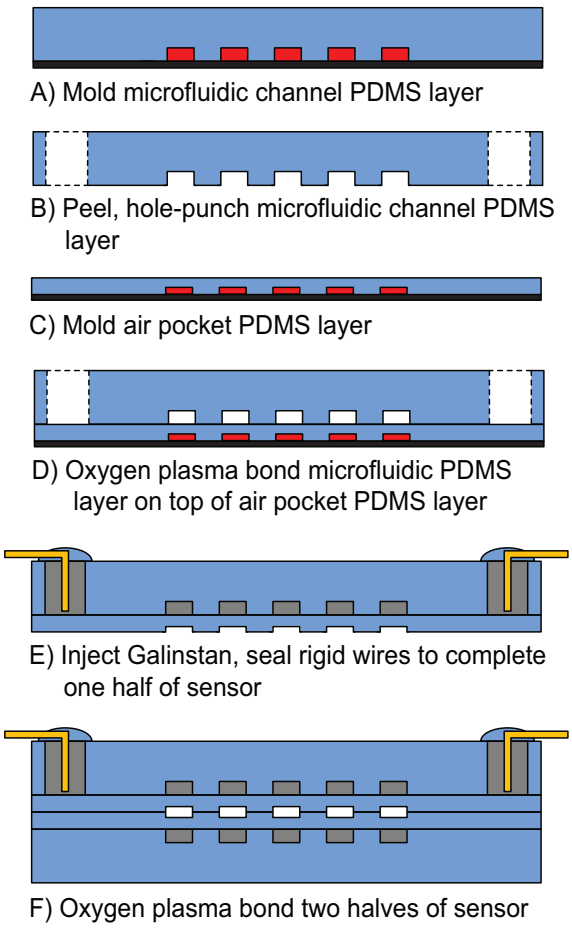

Fig. 2. The fabrication process for a sensor prototype having a 5 × 5 array of capacitive taxels. The 2D schematics correspond to the cross-sectional view at A–A′ in Fig. 1A. (A) The PDMS layer (light blue) having microfluidic channels is created. (B) This layer is peeled from the wafer (black) containing the photoresist master (red) and hole-punched. (C) The PDMS layer having the air pockets is created. (D) The patterned surface of the microchannel layer is O_2 plasma bonded to the exposed surface of the air pocket layer still on the wafer. (E) The bonded layers are peeled from the wafer, and Galinstan (gray) is injected through the hole-punched inlet holes. Rigid wires (yellow) are carefully placed inside the Galinstan-filled inlet and outlet holes. The wires are sealed by pouring uncured PDMS over the holes and then curing the PDMS in an oven. (F) Two separate halves of the sensor are aligned and bonded to create a functional sensor. Wire connects for the bottom PDMS layer are outside the cross-sectional plane and are not shown. *Note*: schematics not drawn to scale. (For interpretation of references to color in this figure legend, the reader is referred to the web version of this article.)

to mimic the mechanical properties of human skin and a liquid metal to serve as flexible plates for the capacitive sensing units. The sensor consists of four layers of PDMS. The two outermost PDMS layers contain microfluidic channels filled with Galinstan, and the two inner layers seal the microfluidic layers and contain an array of square air pockets to tune the overall sensor's mechanical and electrical properties. The microchannels form a 5 × 5 array of taxels connected by in-plane wire paths (lengthways for the top layer and transverse for the bottom layer). The 125 μm thick microchannel wires pass through and connect five 0.5 mm × 0.5 mm taxel plates, each of which is separated from the next plate by 0.5 mm (Fig. 1B). The 5 × 5 array of square air pockets uses the same layout and dimensions as the 5 × 5 array of plates in the microchannel layer.

Soft lithography is a mature microfabrication strategy, but we provide some details specific to our sensor design here. The PDMS masters for the microfluidic layers are fabricated by patterning 40 μm of SU-8 2015 photoresist (Microchem, Newton, MA) onto 4 in. silicon wafers (Fig. 2A). The air pocket layer masters have 18 μm thick SU-8 2010 photoresist (Fig. 2C). The masters are soft baked at 95 °C for 5 min and then exposed to 22.5 mW/cm^2 UV light for 16 s using mylar masks. After a 5 min post-exposure bake on a hot plate at 95 °C, the wafer is developed and then hard baked in an oven at 140 °C for 5 min. The thicknesses of the masters are measured using a profilometer (Dektak IIA, Sloan, Scotia, NY).

We use PDMS with a 10:1 A:B ratio (RTV615, Momentive, Columbus, OH). Each of the two 300 μm thick microfluidic channel layers (Fig. 2A) is fabricated by spin coating PDMS onto the microchannel mold at 500 rpm for 30 s, curing it in an oven at 80 °C for an hour producing a 150 μm thick layer. This process is repeated a second time to produce 300 μm thick PDMS films [7]. The two ends of each wire-plate path are punched with a 700 μm diameter stainless steel TiN-coated round punch (Technical Innovations, Angleton, TX) to create through-holes that serve as inlets and outlets (Fig. 2B) for the injection of Galinstan. The 25 μm thick air pocket layers are created by spinning PDMS onto the master at 3000 rpm for 30 s and curing it in an oven at 80 °C for an hour (Fig. 2C). Each microchannel layer is bound to an air pocket layer (Fig. 2D) after oxygen plasma treatment (PDC-001, Harrick Plasma, Ithaca, NY). We use isopropanol (IPA) to wet each layer and align the PDMS layers under a microscope to ensure accurate alignment of the 5 × 5 arrays of taxel plates and air gaps [34,36]. Each of the two-layer sandwiches is placed on a hot plate at 80 °C for 1 h. We inject the Galinstan into each arm of the five wire-plate paths using a syringe with a 700 μm diameter stainless steel tube attached. Rigid, insulated 500 μm diameter wires are positioned in the inlet and outlet holes and uncured PDMS is poured over the holes. The system is placed in an oven for 2 h at 80 °C to cure the PDMS applied to the channels' inlet and outlet holes. Electrical continuity and resistance of 1.5–2.5 Ω between the inlet and outlet of each wire-plate path are verified with a multimeter. This completes the fabrication of one half of the sensor (Fig. 2E). An O_2 plasma-IPA alignment and bonding technique is used to position and bond two halves of a sensor perpendicular to one another in order to obtain a functional sensor prototype (Fig. 2F).

2.2. Experimental setup and sensor calibration

All experiments were performed with the sensor and its electrical circuit inside a Faraday cage for shielding from external electromagnetic noise. A single taxel was loaded by a uniaxial, point-load using a 1.5 mm × 1.5 mm rectangular-shaped tip (Fig. 3). Double-sided sticky mylar tape was used to affix the sensor to a rigid, flat support plate affixed to a six degree-of-freedom force/torque transducer (Nano-17, ATI Industrial Automation, Apex, NC) having resolutions of 1/80 N and 1/16 N-mm for force and torque, respectively. We validated the calibration of the transducer using known weights.

At the start of each experimental trial, sensor data were collected with the sensor at rest in an unloaded state. The tip of the load platform was then carefully centered over a single taxel with no overlap of adjacent taxel units and placed over the target taxel. Calibrated masses were added to the load platform to gradually achieve a total of 250 g (2.45 N). The actual transmitted load was determined by the force transducer. The masses and load platform were removed in reverse order (and with different load increments) until the sensor was completely unloaded. The sensor was allowed to equilibrate after each change in external load before data were collected for a 0.1 s interval. A total of 20 measurements were made for each of ten independent trials. The sensitivity of two closest neighboring taxels to the loaded taxel was also assessed and is reported here. Eight experimental trials were conducted to assess the effect of surface curvature on sensor performance. Four trials were conducted for each of two sensor configurations: secured to a rigid, flat support plate or secured to a rigid, round support dowel

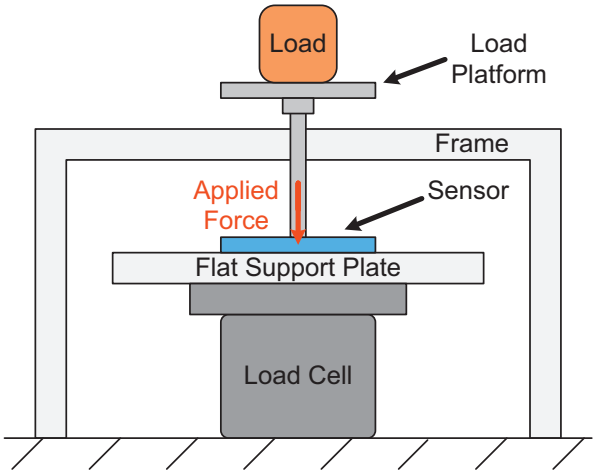

Fig. 3. Experimental setup for point-loading of the microfluidic normal force sensor. The sensor is secured to a rigid, flat support plate that is attached to a load cell. A frame provides support to the slender post of the load platform and allows precise alignment of the tip of the load platform over a single taxel. The flat support plate is replaced with a rigid, round support dowel for assessment of the sensor while wrapped around a curved surface. *Note*: components not drawn to scale.

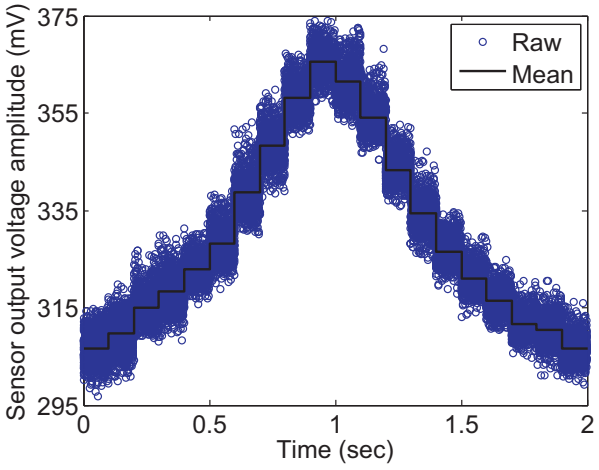

Fig. 4. Sensor output voltage amplitude for a single calibration trial. The raw amplitudes for all cycles of the sinusoidal output signal (circles) and the mean for every 0.1 s interval (line) are shown. Sensor output increased and decreased with loading (0–1 s) and unloading (1–2 s) as expected.

having a curvature similar to that of a human finger. A round acrylic dowel with a radius of 0.635 cm (curvature of 1.575 cm^{-1}) was used as the curved surface.

2.3. Electrical circuitry for data collection

We use a standard charge amplifier circuit to measure the capacitance of individual taxels [37]. An AC input signal is sent through a capacitive sensing unit to the inverting input of an operational amplifier, and the non-inverting input is connected to ground. An external feedback capacitor and resistor are connected across the op amp's inverting input and output. While the input voltage across the external feedback capacitor remains constant, changes in taxel capacitance produces changes in charge, which translates to changes in the op amp's output voltage amplitude [37]. Thus, the gain in amplitude of the AC input signal depends solely on the ratio of capacitance between the constant external capacitor and the variable capacitive sensing unit. Under the assumption of an ideal op amp, nodal analysis can be performed on the circuit to obtain

$$V_{out} = -V_{in}\left(\frac{j\omega R_{out}C_{in}}{j\omega R_{out}C_{out}+1}\right) \quad (1)$$

where V_{out} is the output voltage amplitude, V_{in} is the input voltage amplitude, ω is the excitation frequency of the input signal, R_{out} is the external feedback resistance, C_{in} is the capacitance of a single taxel (connected to the op amp's inverting input), and C_{out} is the external feedback capacitance. If $\omega R_{out}C_{out} \gg 1$, then Eq. (1) simplifies to

$$V_{out} = -V_{in}\frac{C_{in}}{C_{out}} \quad (2)$$

By setting the input signal frequency ω to 62,832 rad/s, R_{out} to 200 MΩ, and C_{out} to 1 pF, the expression $\omega R_{out}C_{out}$ has a value of 12.566 and allows the use of Eq. (2). In response to mechanical deformation under load, changes in taxel capacitance C_{in} can be measured through changes in output voltage amplitude V_{out}. Eq. (2) was confirmed by experimentally measuring V_{out} using known C_{in}, C_{out}, and V_{in} values. This circuit is simple, has relatively fast response time, and filters the output signal to yield a high signal to noise ratio [7,13–15].

We used data acquisition boards (NI-6255 and NI-6211 National Instruments, Austin, TX) to collect data from the load cell at 1 kHz and a single sensor taxel at 200 kHz. The amplifier circuit input signal was sinusoidal with a peak-to-peak voltage of 1 V and frequency of 10 kHz. Sensor taxel data were collected at 20 times the input signal frequency in order to obtain accurate amplitudes from the output signal.

Post-processing of the raw load cell and capacitive sensor signals was performed in Matlab (Mathworks, Natick, MA). The amplitude of the capacitive sensor output voltage was determined for each cycle (using the maximum and minimum value for each wave). The mean load cell readings and mean taxel output amplitudes were computed for each 0.1 s interval of data. Assuming constant V_{in} and C_{out} values, the changes in taxel capacitance C_{in} are directly reflected by changes in output voltage amplitude V_{out} (Eq. (2)). The relative percent change in output voltage amplitude, $\%\Delta V$, was calculated as

$$\%\Delta V = \frac{V_{out,loaded} - V_{out,unloaded}}{V_{out,unloaded}} \times 100\% \quad (3)$$

where the output voltage amplitude V_{out} is a function of load.

3. Results and discussion

Data were collected from individual taxels of a sensor prototype having a 5 × 5 array of capacitive taxels as well as the independent force transducer. The results from ten independent loading and unloading trials are shown first, starting with a brief description of the raw data for one trial. The calibration of the sensor is then presented and fit to a nonlinear model. We use the calibrated sensor to assess the reliability of the sensor's force measurements by comparing them to those of a calibrated load cell. Finally, a brief discussion details the sensor's spatial resolution and robust performance when wrapped around a curved surface.

3.1. Direct point-loading of a single taxel

Fig. 4 shows the raw sensor output voltage amplitudes and mean values for each 0.1 s data collection interval varied with the external load. As expected, an increase in load force resulted in an increase in output voltage amplitude. The spread of amplitude points around the mean is approximately ±7 mV and is due to the low capacitance values being measured (on the order of tenths of pF). Fig. 5 shows the force measured by the sensor as a function of the measured

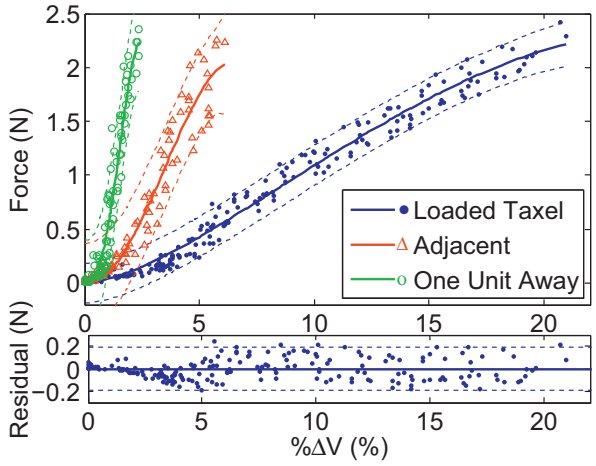

Fig. 5. Sensitivity of taxels to direct and indirect loading. Calibration curves for a directly point-loaded taxel (blue dots and curve fit, Eq. (4)), an adjacent taxel (red triangles and curve fit), and a taxel one unit away (green circles and curve fit) during direct loading of a single taxel. The relative percent changes in output voltage amplitude (data points) were computed using Eq. (3). Regression analysis using the sum of two power functions model was performed to calculate the calibration curves (solid lines) and 95% confidence bounds (dashed lines). The residual plot corresponds to the directly loaded taxel and shows that only 9 of 200 data points fell outside the 95% confidence bounds. Taxel response decreased substantially as distance from the point of load application increased, which suggests that the sensor has a spatial resolution of approximately 0.5 mm. (For interpretation of references to color in this figure legend, the reader is referred to the web version of this article.)

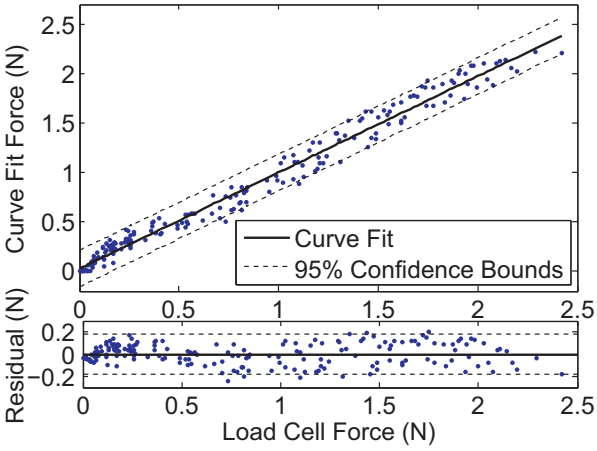

Fig. 6. Comparison of force measurements for a directly loaded taxel as given by the sensor calibration curve and load cell. The relative percent change in output voltage amplitudes was used to calculate curve fit forces F_{fit} (dots) using the calibration equation. The linear regression (solid line; Eq. (5)) revealed a near one-to-one relationship between the microfluidic sensor and load cell measurements. The residual plot shows that only 6 of 200 data points fell outside the 95% confidence bounds (dashed lines).

change in sensor output voltage for ten independent trials on a single taxel under direct point-loading. We fit a power-law curve to the force values as a function of the calculated $\%\Delta V$ using nonlinear regression analysis. The final regression model is given by

$$F_{fit} = 0.0455(\%\Delta V)^{1.73} - 0.00976(\%\Delta V)^{2.14},\ R^2 = 0.982 \quad (4)$$

where F_{fit} is the force calculated by the curve fit. The regression model performs well at both high and low loads. Two power terms were needed to properly fit the nonlinear relationship between load and $\%\Delta V$ at low loads, and to accommodate the slight increase in the linear slope at higher loads (>approx. 1.2 N). Using the power-law fit, the residual plot in Fig. 5 shows that nine data points out of 200 (4.5% of the data) fall outside the 95% confidence interval.

We only present data for loads under 2.5 N. We experimentally determined that a single taxel saturates at roughly a 500 g (4.9 N) load. At this load, the innermost air pocket layers may have collapsed, causing the outermost microfluidic channel layers to touch. At this point, the fluidic capacitive plates would no longer be able to move closer to one another, and the capacitance would achieve a steady state value. It was noted that with masses of 350 g or greater, the small tip of the load platform tended to become misaligned with respect to the target taxel thereby reducing the accuracy of the calibration between the load cell and taxel force readings. Considering the limitations of the experimental setup and our interest in characterizing sensor performance for forces associated with manipulation (approx. 0.15–0.90 N [29]), we used an upper limit of 250 g for the uniaxial loading of a single taxel.

Our sensor response to loading in the 0–2.5 N range is nonlinear at low loads, linear at moderate loads, and slightly nonlinear again at high loads. This nonlinear response can be attributed to many factors associated with the complex mechanical and electrical nature of the device. The primary sources of the nonlinear response are likely the curved deformations of the fluidic capacitance plates and the heterogeneous, deformable dielectric medium consisting of three sub-layers (i.e., two PDMS and one air). This structure and the nonuniform deformation of the capacitor plates result in complex variations in capacitance as the sensor is deformed. In addition, the viscoelastic nature of PDMS is characterized by highly nonlinear stress–strain curves [33,38–40] which could also introduce some nonlinearity into the sensor output. Overall, the nonlinear behavior is a confluence of several physical effects which are difficult to predict with simple analytical models, and so we are investigating these effects further with coupled physics finite element models. Our multilayer sensor exhibits greater sensitivity at low loads, which can be exploited for robotic applications such as semi-autonomous haptic exploration in which light touch is important for the physical examination of objects. The multilayer design enables nonlinear tuning of the sensitivity over a wide range of forces which can be used to tailor the sensor response to the application of interest.

We evaluate the calibration curve fit (Eq. (4)) by directly comparing taxel force measurements to load cell force measurements as shown in Fig. 6. This plot shows that there is nearly perfect agreement between the calibrated sensor and the independently measured load as demonstrated by the linear line having a slope near unity. A linear regression of the taxel's curve fit (F_{fit}) and load cell (F_{LC}) data yielded the following equation:

$$F_{fit} = 0.973F_{LC} + 0.0264, \quad R^2 = 0.9821 \quad (5)$$

The slope and y-intercept had values near one and zero, respectively, indicating that the calibration curve based on the sum of two power functions (Eq. (4)) is effective and that the capacitive sensor can measure forces in the 0–2.5 N range reliably. The 95% confidence bounds (±0.184 N) and residuals were also calculated for the comparison of taxel and load cell force measurements.

Due to the need for dynamic sensing in robotics and other applications, the experimental setup was modified slightly in order to apply a sinusoidal dynamic load to a single taxel. Forces up to approximately 2.5 N were applied at frequencies ranging from 0.4 to 4 Hz. Preliminary results show that sensor output and load cell signals matched well in the loading and unloading phases since no significant lag could be perceived. It is widely known that the fast-adapting type II (FA-II) afferents in the human hand are capable of detecting vibrations ranging from 40 to 400 Hz [41]. Although, vibration detection is beyond the scope of the current prototype, the sensor appears to be capable of measuring low frequency dynamic loads and transient changes in loading, as when contact with an object is being made or released. Such capabilities are similar to those of fast-adapting type I (FA-I) afferents in the

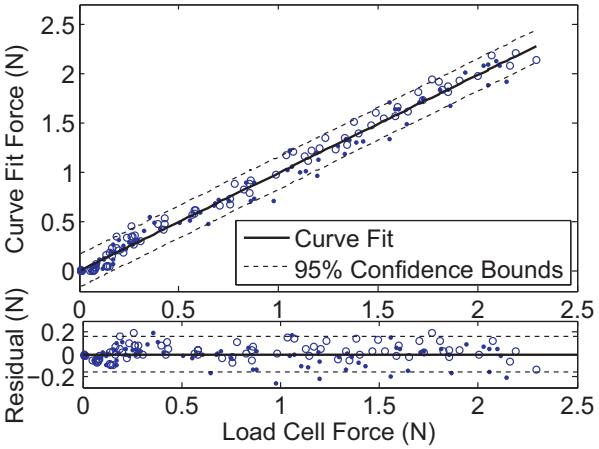

Fig. 7. Assessment of a single taxel's performance on surfaces with different curvatures. Data collected with the sensor attached to a rigid, flat support plate (solid dots) and wrapped around a rigid, round support dowel (open circles) show similar responses. A single calibration curve (Eq. (6)) was used to fit both data sets. A linear regression (solid line, Eq. (7)) revealed a near one-to-one relationship between the microfluidic sensor and load cell measurements. The residual plot shows that 10 of 200 data points fell outside the 95% confidence bounds (dashed lines).

human hand which are maximally sensitive to vibrations ranging from 3 to 40 Hz, although responses to frequencies as low as 0.5 Hz have been reported [42].

3.2. Spatial resolution and robustness to bending

The small tip of the load platform enabled the external load to be centered directly over a single taxel. However, force from the applied load is transmitted to neighboring taxels. To assess the sensitivity of taxels to indirect loading, four experimental trials were conducted for each of the two neighboring taxels: a taxel immediately adjacent to the taxel under direct loading and another taxel one unit away (Fig. 5). As expected, the sensitivity to load for the unloaded taxels decreased with distance from the point of load application. The change in capacitance for a given load is much smaller for the unloaded neighboring taxels than that for the taxel under direct loading (Fig. 5). At a load of 2.25 N, the directly loaded taxel had a $\%\Delta V$ value of 20.26%. The adjacent taxel and the taxel one unit away had $\%\Delta V$ values of 5.59% and 2.15%, respectively, which represent reductions in the $\%\Delta V$ values of 72.4% and 89.4% with respect to the directly loaded taxel. Thus, the sensor prototype has a spatial resolution of approximately 0.5 mm, which would enable precise measurement of bounding areas and center of pressure locations of applied forces.

Fig. 7 shows that the sensor performs similarly and reliably whether mounted to flat or cylindrical support surfaces, suggesting that a single calibration curve might suffice. As with the flat surface condition, a sum of two power functions fit the data from the curved surface condition well. The calibration curve for data pooled from the flat and curved surface conditions and the linear regression of the taxel's curve fit and load cell data are given by the following equations, respectively,

$$F_{fit} = -0.478(\%\Delta V)^{2.00} + 0.506(\%\Delta V)^{1.98}, \quad R^2 = 0.986 \tag{6}$$

$$F_{fit} = 0.99F_{LC} - 0.00454, \quad R^2 = 0.986 \tag{7}$$

The 95% confidence bounds (±0.165 N) show a force range similar to the one obtained from the previously calibrated taxel (Fig. 6). No major performance difference was observed, suggesting that this particular sensor prototype functions similarly, regardless of surface curvature. This finding is likely related to the dimensional relationships between the individual taxels, their spacing, and the curvature of the round support dowel. If small enough, a taxel will act as if mounted to flat surface because even a curved surface will appear locally flat. In addition to the presented results, testing was performed on surfaces with larger curvatures to see if any curvature limits could be detected. The sensor was wrapped around four dowels with radii of 0.397 cm, 0.318 cm, 0.238 cm, and 0.159 cm (curvatures of 2.519 cm^{-1}, 3.145 cm^{-1}, 4.202 cm^{-1}, and 6.289 cm^{-1}, respectively). The sensor tolerated the increased curvature and remained functional as force was applied on a single taxel, further supporting the findings from the finger-sized dowel. These results show that this multilayer microfluidic tactile sensor is flexible and functions well on surfaces having curvatures consistent with artificial fingers and much higher.

4. Summary

In this work, we have created a functional prototype of a microfluidic normal force sensor that uses a liquid metal alloy for its internal circuitry. The novel use of conductive fluids as deformable capacitive plates and wire paths offers significant advantages over the use of standard solid components such as robustness to cracking and fatigue. The multilayer design utilizing PDMS and air sub-layers allows for the tuning of mechanical and electrical properties, particularly for the heterogeneous, deformable dielectric medium. The sensor also offers advantages such as ease of fabrication, low cost and non-toxic components, large degree of flexibility, robustness, and repeatable measurements. Our work expands the design space for flexible MEMS sensors by demonstrating that liquid metal alloys such as Galinstan can be used as both flexible capacitor plates and wire paths [20,21]. Our microfluidic PDMS sensor remained functional after being wrapped around a surface having a small curvature similar to that of a human finger and showed indications of being capable of measuring low frequency dynamic loads. Additional testing is needed to determine whether the sensor remains functional despite twisting and stretching. Our sensor performed reliably during static loading and unloading trials for forces up to 2.5 N and exhibited 0.5 mm spatial resolution. A functional artificial sensor skin would consist of a larger sensor (8 in. wafers are state of the art) or several of these sensor prototypes covering a large area. Sensing units and sensor resolution can be modified according to the surface area and application of interest.

The primary motivation for this work is tactile sensing for robotics applications. Our current experimental setup and prototype are not well suited for complete dynamic analysis and shear force measurements required for use on an artificial hand. However, it reliably measures normal forces with a spatial resolution appropriate for artificial grasping, is robust, and is flexible in order to be conformally wrapped around curved objects such as artificial fingers. The deformable elastomeric skin could enhance grip by cushioning impacts, increasing the effective contact area, and increasing friction at the hand-object interface during grasp. The sensor's nonlinear response, which can be attributed to its complex mechanical and electrical design, is advantageous for tactile sensing due to its greater sensitivity at low loads and ability to withstand large force ranges. The multilayer design can be modified to tune the nonlinear sensor response according to application-specific design criteria. In addition, MEMS applications that require sensors capable of withstanding elastic deformations, such as bending and stretching, could benefit from replacing rigid metal components with conductive fluids, as described in this work. While the sensor skin was initially conceived for robotic hands, the sensor could easily be applied to other robotic and haptic applications. For instance, the skin could be applied to large surface areas (e.g., wrapped around robot arms [43]) for safe human-robot interactions, or applied to human-machine interfaces for haptic applications.

Our future work will focus first on enhancing the experimental setup for complete dynamic characterization of the sensor skin. We will also implement multiplexing of the data collection circuitry to enable simultaneous measurement of signals from multiple taxels to identify features of loads such as center of pressure location. In addition, coupled physics finite element models will be developed such that the sensor design (e.g., thickness of PDMS layers, dimensions and placement of air pockets, etc.) can be tuned for specific sensing design requirements (e.g., range, dynamic response). Previous works [15,44] have demonstrated that arrays of normal force sensing units can be used to approximate shear by simply adding bumps or pillars on the exposed PDMS surface and looking at the relative signal response between adjacent sensing elements. Similar strategies could be attempted with our microfluidic force sensor to expand the sensing capabilities to include shear forces.

Acknowledgments

This material is based upon work supported by the National Science Foundation under Grant No. 0954254. Any opinions, findings, and conclusions or recommendations expressed in this material are those of the authors and do not necessarily reflect the view of the National Science Foundation. The authors would also like to thank Dr. Philip Wheat and Dr. Steven Klein who assisted with clean room and microfabrication training, as well as Charles Corredor who helped with the Faraday cage experimental setup. In addition, the authors appreciate the help of Randall Hellman for the dynamic loading setup and Asuka Nakano for the Japanese literature review.

References

[1] H. Yousef, M. Boukallel, K. Althoefer, Tactile sensing for dexterous in-hand manipulation in robotics—a review, Sens. Actuators A: Phys. 167 (2011) 171–187.
[2] J.M. Engel, N. Chen, K. Ryu, S. Pandya, C. Tucker, Y. Yang, C. Liu, Multi-layer embedment of conductive and non-conductive PDMS for all-elastomer MEMS, in: Proceedings of the International Conference on Solid-State Sensors, Actuators and Microsystems, 2006, pp. 316–319.
[3] Z.-M. Dang, M.-J. Jiang, D. Xie, S.-H. Yao, L.-Q. Zhang, J. Bai, Supersensitive linear piezoresistive property in carbon nanotubes/silicone rubber nanocomposites, J. Appl. Phys. 104 (2008), 024114.
[4] L. Ventrelli, L. Beccai, V. Mattoli, A. Menciassi, P. Dario, Development of a stretchable skin-like tactile sensor based on polymeric composites, in: Proceedings of IEEE International Conference on Robotics and Biomimetics, 2009, pp. 123–128.
[5] A.P. Micolich, L.L. Bell, A.R. Hamilton, An improved process for fabricating high-mobility organic molecular crystal field-effect transistors, J. Appl. Phys. 102 (2007) 084511.
[6] T. Adrega, S. Lacour, Stretchable gold conductors embedded in PDMS and patterned by photolithography: fabrication and electromechanical characterization, J. Micromech. Microeng. 20 (2010) 055025.
[7] H.-K. Lee, S.-I. Chang, E. Yoon, A flexible polymer tactile sensor: fabrication and modular expandability for large area deployment, J. Microelectromech. Syst. 15 (2006) 1681–1686.
[8] J.-T. Feng, Y.-P. Zhao, Influence of different amount of Au on the wetting behavior of PDMS membrane, Biomed. Microdev. 10 (2007) 65–72.
[9] G.P. Zhang, Z.G. Wang, Fatigue of small-scale metal materials: from micro-to nano-scale, in: G.C. Sih (Ed.), Multiscale Fatigue Crack Initiation and Propagation of Engineering Materials: Structural Integrity and Microstructural Worthiness, Springer Science+Business Media, New York, 2008, pp. 275–326.
[10] D.-H. Kim, J. Song, W.M. Choi, H.-S. Kim, R.-H. Kim, Z. Liu, Y.Y. Huang, K.-C. Hwang, Y.-W. Zhang, J.A. Rogers, Materials and noncoplanar mesh designs for integrated circuits with linear elastic responses to extreme mechanical deformations, Proc. Natl. Acad. Sci. 105 (2008) 18675–18680.
[11] M.-Y. Cheng, C.-M. Tsao, Y.-Z. Lai, Y.-J. Yang, The development of a highly twistable tactile sensing array with stretchable helical electrodes, Sens. Actuators A: Phys. 166 (2011) 226–233.
[12] B.L. Gray, R.S. Fearing, A surface micromachined microtactile sensor array, in: Proceedings of IEEE International Conference on Robotics and Automation, vol. 1, 1996, pp. 1–6.
[13] M. Sergio, N. Manaresi, M. Tartagni, R. Guerrieri, R. Canegallo, A textile-based capacitive pressure sensor, in: Proceedings of IEEE International Conference on Sensors, vol. 2, 2002, pp. 1625–1630.
[14] M.J. Da Silva, E. Schleicher, U. Hampel, Capacitance wire-mesh sensor for fast measurement of phase fraction distributions, Meas. Sci. Technol. 18 (2007) 2245–2251.
[15] H.-K. Lee, J. Chung, S.-I. Chang, E. Yoon, Normal and shear force measurement using a flexible polymer tactile sensor with embedded multiple capacitors, J. Microelectromech. Syst. 17 (2008) 934–942.
[16] K.-H. Kim, Y.H. Seo, Proofmass-less vibration sensor using the motion of self-charged anion and cation in an electrolyte for ultra-high frequency detection, in: Proceedings of IEEE International Conference on Micro Electro Mechanical Systems, Tucson, AZ, USA, 2008, pp. 94–97.
[17] W.-Y. Tseng, J.S. Fisher, J.L. Prieto, K. Rinaldi, G. Alapati, A.P. Lee, A slow-adapting microfluidic-based tactile sensor, J. Micromech. Microeng. 19 (2009) 085002.
[18] N. Wettels, V.J. Santos, R.S. Johansson, G.E. Loeb, Biomimetic tactile sensor array, Adv. Robot. 22 (2008) 829–849.
[19] N. Wettels, L.M. Smith, V.J. Santos, G.E. Loeb, Deformable skin design to enhance response of a biomimetic tactile sensor, in: Proceedings of IEEE International Conference on Biomedical Robotics and Biomechatronics, 2008, pp. 132–137.
[20] H.-J. Kim, C. Son, B. Ziaie, A multiaxial stretchable interconnect using liquid-alloy-filled elastomeric microchannels, Appl. Phys. Lett. 92 (2008) 011904.
[21] H. Hu, K. Shaikh, C. Liu, Super flexible sensor skin using liquid metal as interconnect, in: Proceedings of IEEE International Conference on Sensors, 2007, pp. 815–817.
[22] P. Surmann, H. Zeyat, Voltammetric analysis using a self-renewable non-mercury electrode, Anal. Bioanal. Chem. 383 (2005) 1009–1013.
[23] Galinstan MSDS, Geratherm Medical AG, Geschwenda, Germany, September 14, 2006.
[24] D. Schulze, C. Karcher, V. Kocourek, J.U. Mohring, Electrically induced instabilities of liquid metal free surfaces, in: 4th International Scientific Colloqium on Modelling for Material Processing, Riga, Latvia, 2006, pp. 50–55.
[25] Y.-L. Park, C. Majidi, R. Kramer, P. Bérard, R.J. Wood, Hyperelastic pressure sensing with a liquid-embedded elastomer, J. Micromech. Microeng. 20 (2010) 125029.
[26] C. Majidi, R. Kramer, R.J. Wood, A non-differential elastomer curvature sensor for softer-than-skin electronics, Smart Mater. Struct. 20 (2011) 105017.
[27] R.K. Kramer, C. Majidi, R. Sahai, R.J. Wood, Soft curvature sensors for joint angle proprioception, in: Proceedings of the IEEE/RSJ International Conference on Intelligent Robots and Systems, San Francisco CA, USA, 2011, pp. 1919–1926.
[28] V. Maheshwari, R. Saraf, Tactile devices to sense touch on a par with a human finger, Angew. Chem. Int. Ed. 47 (2008) 7808–7826.
[29] R. Dahiya, G. Metta, M. Valle, G. Sandini, Tactile sensing—from humans to humanoids, IEEE Trans. Robot. 26 (2010) 1–20.
[30] P. Peng, R. Rajamani, A.G. Erdman, Flexible tactile sensor for tissue elasticity measurements, J. Microelectromech. Syst. 18 (2009) 1226–1233.
[31] H.B. Muhammad, C. Recchiuto, C.M. Oddo, L. Beccai, C.J. Anthony, M.J. Adams, M.C. Carrozza, M.C.L. Ward, A capacitive tactile sensor array for surface texture discrimination, Microelectron. Eng. 88 (2011) 1811–1813.
[32] C. Liu, Recent developments in polymer MEMS, Adv. Mater. 19 (2007) 3783–3790.
[33] F. Schneider, T. Fellner, J. Wilde, U. Wallrabe, Mechanical properties of silicones for MEMS, J. Micromech. Microeng. 18 (2008) 065008.
[34] B.H. Jo, L.M. Van Lerberghe, K.M. Motsegood, D.J. Beebe, Three-dimensional micro-channel fabrication in polydimethylsiloxane (PDMS) elastomer, J. Microelectromech. Syst. 9 (2000) 76–81.
[35] J.C. Lotters, W. Olthuis, P.H. Veltink, P. Bergveld, The mechanical properties of the rubber elastic polymer polydimethylsiloxane for sensor applications, J. Micromech. Microeng. 7 (1997) 145–147.
[36] S. Li, S. Chen, Polydimethylsioxane fluidic interconnects for microfluidic systems, IEEE Trans. Adv. Packag. 26 (2003) 242–247.
[37] W.G. Jung, Op Amp Applications Handbook, Newnes, Massachusetts, USA, 2005.
[38] J.E. Mark, Physical Properties of Polymers Handbook, Springer Science+Business Media, New York, USA, 2007.
[39] K. Khanafer, A. Duprey, M. Schlicht, R. Berguer, Effects of strain rate, mixing ratio, and stress–strain definition on the mechanical behavior of the polydimethylsiloxane (PDMS) material as related to its biological applications, Biomed. Microdev. 11 (2008) 503–508.
[40] A. Goyal, A. Kumar, P.K. Patra, S. Mahendra, S. Tabatabaei, P.J.J. Alvarez, G. John, P.M. Ajayan, In situ synthesis of metal nanoparticle embedded free standing multifunctional PDMS films, Macromol. Rapid Commun. 30 (2009) 1116–1122.
[41] R.S. Johansson, J.R. Flanagan, Tactile sensory control of object manipulation in humans, in: J.H. Kaas, E. Gardner (Eds.), Handbook of the Senses, Academic Press, San Diego, 2008, pp. 67–86.
[42] L.A. Jones, S.J. Lederman, Human Hand Function, Oxford University Press, New York, USA, 2006.
[43] T. Mukai, M. Onishi, T. Odashima, S. Hirano, Z. Luo, Development of the tactile sensor system of a human–interactive robot "RI-MAN", IEEE Trans. Robot. 24 (2008) 505–512.
[44] S. Koterba, Y. Matsuoka, A triaxial force discernment algorithm for flexible, high density, artificial skin, in: Proceedings of IEEE International Conference on Robotics and Automation, 2006, pp. 1359–1364.
[45] Y.-L. Park, B.-R. Chen, R.J. Wood, Soft Artificial Skin with Multi-Modal Sensing Capability Using Embedded Liquid Conductors, IEEE Sensors Conference, Limerick, Ireland, 2011.

Biographies

Ruben D. Ponce Wong obtained his B.S. degree in Bioengineering at Arizona State University in May 2008. He is currently in the Mechanical Engineering Ph.D. program

at the same institution. His work focuses on the fabrication of microfluidic tactile sensors and employment of machine learning techniques to map tactile sensor data to object properties. He received an Arizona State University Graduate Fellowship in Spring 2011.

Jonathan D. Posner is an associate professor in mechanical engineering and adjunct professor chemical engineering at University of Washington (UW). He came to UW from Arizona State University where he was an associate professor of mechanical and chemical engineering and continues his role as adjunct faculty in the Consortium for Science, Policy, & Outcomes (CSPO). Dr. Posner earned his Ph.D. (2001) degree in Mechanical Engineering at the University of California, Irvine. He spent 18 months as a fellow at the von Karman Institute for Fluid Mechanics in Rhode Saint Genèse, Belgium and two years as a postdoctoral fellow at the Stanford University. His interests include micro/nanofluidics, sensors, electrokinetics, electrochemistrys, self-assembly of colloids, and the physics of nanoparticles at interfaces. At CSPO, Posner has interest in the social implications of technology, role of science in policy and regulation, as well as ethics education. Dr. Posner is a Washington State 'STAR' professor, was honored with a 2008 NSF CAREER award for his work on the physics of self-assembly of nanoparticles at fluid–solid and fluid–fluid interfaces. He has also been recognized for his Excellence in Experimental Research by the von Karman Institute for Fluid Dynamics.

Veronica J. Santos is an Assistant Professor of Mechanical and Aerospace Engineering and Graduate Faculty of Bioengineering at Arizona State University. She received the B.S. degree in mechanical engineering with a music minor from the University of California at Berkeley in 1999, and the M.S. and Ph.D. degrees in mechanical engineering with a biometry minor from Cornell University in 2004 and 2007, respectively. From 2007 to 2008, she was a postdoctoral research associate at the Alfred E. Mann Institute for Biomedical Engineering at the University of Southern California where she worked on a team to develop a biomimetic tactile sensor for prosthetic hands. Her research interests include hand biomechanics, neural control of movement, robotics, prosthetics, and tactile sensors for the development of human–machine systems for grasp and dexterous manipulation. Dr. Santos was awarded a 2010 NSF CAREER award for work to develop bio-inspired control policies for robotic hands, selected to participate in the 2010 National Academy of Engineering Frontiers of Engineering Education Symposium and selected as a 2012 Lindseth Lecturer by the Sibley School of Mechanical and Aerospace Engineering at Cornell University.